Shock waves: The Maxwell-Cattaneo case

F. J. Uribe

Department of Physics, Universidad Autónoma Metropolitana, Avenida San Rafael Atlixco 186, Mexico City 09340, Mexico

(Received 4 May 2015; revised manuscript received 10 December 2015; published 11 March 2016)

Several continuum theories for shock waves give rise to a set of differential equations in which the analysis of the underlying vector field can be done using the tools of the theory of dynamical systems. We illustrate the importance of the divergences associated with the vector field by considering the ideas by Maxwell and Cattaneo and apply them to study shock waves in dilute gases. By comparing the predictions of the Maxwell-Cattaneo equations with shock wave experiments we are lead to the following conclusions: (a) For low compressions (low Mach numbers: M) the results from the Maxwell-Cattaneo equations provide profiles that are in fair agreement with the experiments, (b) as the Mach number is increased we find a range of Mach numbers ($1.27 \approx M_1 < M < M_2 \approx 1.90$) such that numerical shock wave solutions to the Maxwell-Cattaneo equations cannot be found, and (c) for greater Mach numbers ($M > M_2$) shock wave solutions can be found though they differ significantly from experiments.

DOI: 10.1103/PhysRevE.93.033110

I. INTRODUCTION

The Navier-Stokes equations [1–3] give a sound hydrodynamic description whose thermodynamical content is given by linear irreversible thermodynamics (LIT) [4]. However, the shock wave profiles given by the Navier-Stokes equations are thinner than the experimental and simulated profiles especially for strong shocks [5] (see also Fig. 6). While there is a vast amount of information on shock waves [2,3,6], the search for alternative hydrodynamic theories that can improve the shock wave profiles predicted by the Navier-Stokes equations has been active for several decades. Among the several hydrodynamic alternatives to the Navier-Stokes equations, the Maxwell-Cattaneo equations are at the core of extended irreversible thermodynamics (EIT) [7] which extends LIT. Therefore, it is natural to ask what are the predictions of the Maxwell-Cattaneo equations for shock wave phenomena, and this point is addressed here.

In a previous work [8] we considered the relaxation ideas by Maxwell-Cattaneo with the addition of anisotropic temperatures and heat conduction for dense fluids [9]. Here we consider only one temperature and isotropic heat conduction for dilute monoatomic gases. The case of dilute gases leaves out important applications but provides explicit expressions for the transport coefficients [10] and relaxation times [7,11], and therefore one is not forced to make guesses on these quantities. Besides, a sound theory should give, we think, the simpler cases correctly (like the dilute gas). The partial number of references dealing with shock waves in dilute gases that we give here [5–7,11–49] reflects in part that we are far from having a consensus on the phenomenon even in dilute gases. As we will show, the results from the Maxwell-Cattaneo equations for shock waves are in fair agreement with experiments for Mach numbers near 1—the Mach number (M) is defined at the cold (lower temperature) equilibrium part of the shock, as the quotient of the (supersonic) shock wave to sound velocities—but fail for Mach numbers of order 2 or above. Even for Mach numbers as low as 1.35 we have been unable to find shock wave solutions to the Maxwell-Cattaneo equations, and a simple geometrical explanation for why this happens is given.

In 1867 Maxwell [50] pointed out that for a solid the stress tensor (denoted here by $\boldsymbol{\sigma}$) is proportional to the strain or deformation tensor (denoted by $\boldsymbol{\epsilon}$), while for fluids the stress is proportional to the strain rate $\boldsymbol{\sigma} \sim \eta \frac{d\boldsymbol{\epsilon}}{dt}$. Maxwell argued that when both behaviors are present the following is to be expected,

$$\boldsymbol{\sigma} + \tau_\sigma \dot{\boldsymbol{\sigma}} \sim \eta \dot{\boldsymbol{\epsilon}}. \tag{1}$$

Here η is the viscosity, τ_σ a relaxation time [50] which for air is typically hundreds of picoseconds, and the superior dots represent the comoving (total, material) time derivative (a point discussed further below).

For the Maxwell model with the comoving derivative we have that

$$\frac{4}{3}\eta \frac{dv}{dx} = \sigma + \tau_\sigma \left[\frac{\partial \sigma}{\partial t} + v \frac{\partial \sigma}{\partial x} \right] \approx \sigma(x + \tau_\sigma v, t + \tau_\sigma), \tag{2}$$

where we assumed that $\tau_\sigma v$ and τ_σ are small so that it is not necessary to include more terms in the Taylor series for $\sigma(x + \tau_\sigma v, t + \tau_\sigma)$. The factor $4/3$ on the left-hand side of the previous equation is needed to reproduce the Navier-Stokes expression for the pressure tensor corresponding to a plane wave in three dimensions when $\tau_\sigma \to 0$. The interpretation of Eq. (2) is as follows [3,9]: the inhomogeneity of the hydrodynamics velocity ("cause") has the "effect" of producing a stress; Eq. (2) shows that there is a time delay and space shift between the "cause" and the "effect." This is in contrast with the Navier-Stokes equations that assume that the "effect" happens at the same position and time as the "cause." The previous argument supports the use of the comoving derivative; another argument is that the expression for σ is Galilean invariant.

Later on, in 1958, Cattaneo [51] argued that the Fourier law for heat conduction should be modified, in order to avoid infinite velocity propagation of heat flow implied by the diffusion equation. Cattaneo's approach [51] can be written in a form like Maxwell's, but with a partial derivative with respect to time (fixed in space) rather than a comoving time derivative. The use of either a temporal partial derivative or a comoving one is the subject of controversies [8,52] and there is a work pointing out that the use of the partial time derivative gives rise to a paradox [53] in heat conduction phenomena which is solved when one uses the comoving derivative; this

supports the use of it. However, the theory resulting from using the comoving derivative apparently has not been tested for the shock wave case, so that there is no guarantee that the paradox-free alternative is physically sound in this case. In this work we will use the comoving time derivative, that is,

$$\mathbf{Q} + \tau_Q \dot{\mathbf{Q}} = -\kappa \nabla T, \tag{3}$$

where $\mathbf{Q}$ is the heat flow, τ_Q a relaxation time, κ the thermal conductivity, and T the temperature. The use of a partial derivative with respect to time instead of the material derivative in the term including the relaxation time, in both Maxwell and Cattaneo relaxation equations, makes no contribution (different from the Navier-Stokes equations) at all in stationary steady-state problems such as the structure of a steady fluid shock wave.

A similar analysis to the one done for the stress holds for the heat flux; see Eq. (2). The time delay for the heat flux gives rise to second sound [7,52] (heat waves) that has been observed in experiments, and space shift is observed in molecular dynamics simulations for dense gases [9]. If the partial derivative of the stress or of the heat flux is used instead of the comoving derivative, then there will be a time delay but not a space shift.

Maxwell's viscoelastic model and Cattaneo's modification of Fourier law have been driving forces for several theories; some of them are grouped under the term extended irreversible thermodynamics that actually encompasses several alternatives [7,11,49,54]. Other approaches for extending irreversible thermodynamics beyond the linear regime are available [54–65], though the list is not complete. We will leave out some thermodynamic considerations in the shock front (the region between the two equilibrium states of the shock wave [6]) such as entropy production; the reason is that our results are independent of the explicit use of them and we would like to keep the hypotheses to a minimum to get a clearer picture. In the last section we will comment on such concepts. For shock waves and other cases in dilute gases, moment methods [12,15–22,66–69] for solving the Boltzmann equation are akin to Maxwell's and Cattaneo's ideas; for a partial list of works dealing with shock waves in dilute gases see the references in [5,6,12,15–49]. Several of the theories that use moment methods have an upper bound for the Mach number above which solutions of the shock wave problem do not exist [12,15–19] and as more moments are included the analysis of the underlying dynamical system becomes intricate [12]. As we will illustrate with the simple relaxation model used here, nonexistence of solutions for some moment methods may be understood in terms of the singularities of the underlying dynamical system.

The main objective of this work is to elucidate the limitations of relaxation equations *à la* Maxwell-Cattaneo for shock waves by considering the profiles and the solution curves of the model (*orbits* in the mathematical jargon); this is mainly accomplished by comparing with experimental information, but we consider also the direct simulation Monte Carlo (DSMC) method. In addition, we use the corresponding state principle (CSP) as a source for the transport coefficients needed to solve the differential equations considered in this work and we also use the "soft sphere" model that is used in many studies on shock waves. Another objective is to provide a geometrical argument that allows us to understand in simple terms why the Maxwell-Cattaneo equations do not have shock wave solutions in some cases, and to give some physical arguments of why this happens. Other minor results are mentioned, such as the fact that the solution curves of the dynamical system that result from using the ideas by Maxwell-Cattaneo are independent of the interaction potential, as happens for the Navier-Stokes equations [6,12,13].

In what follows we discuss the conservation equations and define reduced variables to obtain the differential equations to be solved in Sec. II. In Sec. III we compare the different profiles obtained using theoretical equations, experiments (when available), and simulations. In the last section we provide some final remarks.

II. CONSERVATION EQUATIONS AND THE DYNAMICAL SYSTEM

Conservation of mass, momentum, and energy imply that for a steady plane shock wave propagating along the x direction with velocity $\mathbf{v}(\mathbf{r},t) = v(x)\mathbf{i}$ [8,10,32],

$$\rho v = c_1, \tag{4a}$$

$$P_{xx} + \rho v^2 = \frac{2}{3}\rho e - \sigma + \rho v^2 = c_2, \tag{4b}$$

$$\rho v\left[e + \frac{P_{xx}}{\rho} + \frac{v^2}{2}\right] + Q = \rho v\left[e + \frac{\frac{2}{3}\rho e - \sigma}{\rho} + \frac{v^2}{2}\right] + Q = c_3, \tag{4c}$$

with $c_i, i = 1,2,3$, constants that can be expressed in terms of the values for the density $\rho \equiv \rho(x)$, temperature $T \equiv T(x)$, and velocity $v \equiv v(x)$ at either end of the shock. In addition, the xx component of the pressure tensor $[P_{xx} \equiv P_{xx}(x)]$, the specific internal energy $[e \equiv e(x)]$, and the heat flux $\mathbf{Q}(\mathbf{r},t)$ are given by

$$P_{xx} = \frac{2}{3}\rho e - \sigma, \quad e = \frac{3}{2}\frac{k_B}{m}T, \quad \mathbf{Q}(\mathbf{r},t) = Q(x)\mathbf{i} \equiv Q\mathbf{i}, \tag{5}$$

where k_B is the Boltzmann constant and m the particle mass. For dilute monoatomic gases the thermal conductivity can be expressed in terms of the viscosity (first Sonine approximation [10]), and the two relaxation times are known [7,11],

$$\kappa = \frac{15}{4}\frac{k_B \eta}{m}, \quad \tau_\sigma = \frac{m\eta}{k_B \rho T}, \quad \tau_Q = \frac{2}{5}\frac{\kappa m^2}{\rho k_B^2 T} = \frac{3}{2}\tau_\sigma, \tag{6}$$

where the temperature dependence of the viscosity (η) is not specified for the moment. The first Sonine approximation gives a Prandtl number of value $\mathrm{Pr} = 2/3$. The conservation equations, Eqs. (4), should be supplemented by the steady Maxwell and Cattaneo relaxation equations, see Eqs. (2) and (3),

$$\sigma + \tau_\sigma v\frac{d\sigma}{dx} = \frac{4}{3}\eta\frac{dv}{dx}, \tag{7a}$$

$$Q + \tau_Q v\frac{dQ}{dx} = -\kappa\frac{dT}{dx}. \tag{7b}$$

It is convenient to consider dimensionless variables; they are defined as follows: let v_0 be the velocity at the cold

part of the shock, and define a reduced velocity, a reduced temperature, a reduced distance, a reduced viscosity, and a reduced thermal conductivity by

$$v^\star(s) \equiv v(x)/v_0, \quad T^\star(s) \equiv k_B T(x)/mv_0^2, \quad s \equiv x/\lambda, \\ \lambda \equiv \frac{4}{3}\frac{\eta_0}{\rho_0 v_0}, \quad \eta^\star \equiv \eta/\eta_0, \quad \kappa^\star \equiv \kappa/\kappa_0, \tag{8}$$

where ρ_0, η_0, and κ_0 are respectively, the mass density, viscosity, and thermal conductivity evaluated at the cold part of the shock. The choice of λ is for convenience in order to have a simple form of the reduced Navier-Stokes equations [see Eqs. (16)]: its relation to the mean-free path is given in Sec. III.

The conservation equations (4a)–(4c) depend on the three conservation parameters c_i whose values are the following,

$$c_1 = \rho_0 v_0, \quad c_2 = \rho_0 v_0^2(1+T_0^\star), \quad c_3 = \rho_0 v_0{}^3\left(\tfrac{5}{2}T_0^\star + \tfrac{1}{2}\right), \tag{9}$$

with $T_0^\star$ the reduced temperature at the cold part of the shock. It can be related to the Mach number (M) at the cold part of the shock,

$$M = \sqrt{\frac{3}{5\,T_0^\star}}, \tag{10}$$

or to the compression factor through the use of the Rankine-Hugoniot jump conditions given below.

We now explain how the differential equations for the velocity and temperature are obtained. Conservation of mass gives $\rho(x) = c_1/v(x)$ so that we can always replace $\rho(x)$ in terms of $v(x)$. Conservation of momentum and energy then give the following expressions for the viscous stress tensor and the heat flux,

$$\sigma = \frac{Tc_1k_B + c_1v^2m - c_2vm}{vm}, \tag{11a}$$

$$Q = c_3 - \frac{3}{2}\frac{c_1k_BT}{m} + \frac{1}{2}c_1v^2 - c_2v \\ = c_3 - \frac{3}{2}v\sigma + 2c_1v^2 - \frac{5}{2}c_2v. \tag{11b}$$

When Eq. (11a) is substituted into Maxwell's relaxation equation, and the first equality that appears in Eq. (11b) is substituted into Cattaneo's relaxation equation, we obtain

$$\frac{c_1k_BT}{vm} + c_1v - c_2 - \frac{\tau_\sigma c_1k_BT\frac{dv}{dx}}{vm} + \frac{\tau_\sigma c_1k_B\frac{dT}{dx}}{m} + \tau_\sigma vc_1\frac{dv}{dx} = \frac{4}{3}\eta\frac{dv}{dx}, \tag{12a}$$

$$c_3 - \frac{3}{2}\frac{c_1k_BT}{m} + \frac{1}{2}c_1v^2 - c_2v + \tau_Q v^2c_1\frac{dv}{dx} - \tau_Q vc_2\frac{dv}{dx} - \frac{3}{2}\frac{\tau_Q vc_1k_B\frac{dT}{dx}}{m} = -\kappa\frac{dT}{dx}. \tag{12b}$$

In terms of reduced variables and using $\tau_\sigma = \frac{\eta v^\star}{\rho_0 v_0^2 T^\star}$, $\tau_Q = 3\tau_\sigma/2$, and $\frac{ds}{dx} = 1/\lambda = (3\rho_0 v_0)/4\eta_0$, the reduced form of Eqs. (12a) and (12b) is

$$\frac{\rho_0v_0k_B\frac{mv_0^2T^\star}{k_B}}{v_0v^\star m} + \rho_0v_0^2v^\star - \rho_0v_0^2(1+T_0^\star) - \frac{\left(\frac{\eta v^\star}{\rho_0v_0^2T^\star}\right)\rho_0v_0k_B\frac{mv_0^2T^\star}{k_B}v_0\frac{dv^\star}{ds}\frac{ds}{dx}}{v_0v^\star m} \\ + \frac{\left(\frac{\eta v^\star}{\rho_0v_0^2T^\star}\right)\rho_0v_0k_B\frac{mv_0^2}{k_B}\frac{dT^\star}{ds}\frac{ds}{dx}}{m} + \left(\frac{\eta v^\star}{\rho_0v_0^2T^\star}\right)\rho_0v_0^2v^\star v_0\frac{dv^\star}{ds}\frac{ds}{dx} = \frac{4}{3}\eta v_0\frac{dv^\star}{ds}\frac{ds}{dx}$$

or

$$\left[\frac{3\eta^\star}{4}\left(\frac{v^{\star2}}{T^\star} - 1\right) - \eta^\star\right]\frac{dv^\star}{ds} + \frac{3\eta^\star}{4}\frac{v^\star}{T^\star}\frac{dT^\star}{ds} + \frac{T^\star}{v^\star} + v^\star - (1+T_0^\star) = 0, \tag{13a}$$

and

$$\frac{\rho_0v_0^3}{2}(5T_0^\star+1) - \frac{3}{2}\frac{\rho_0v_0k_B\frac{mv_0^2T^\star}{k_B}}{m} + \frac{1}{2}\rho_0v_0^3v^\star - \rho_0v_0^2(1+T_0^\star)v_0v^\star + \left(\frac{3\eta v^\star}{2\rho_0v_0^2T^\star}\right)v_0^2v^{\star2}\rho_0v_0v_0\frac{dv^\star}{ds}\frac{ds}{dx} \\ - \left(\frac{3\eta v^\star}{2\rho_0v_0^2T^\star}\right)v_0v^\star\rho_0v_0^2(1+T_0^\star)v_0\frac{dv^\star}{ds}\frac{ds}{dx} - \frac{3}{2m}\left(\frac{3\eta v^\star}{2\rho_0v_0^2T^\star}\right)v_0v^\star\rho_0v_0k_B\left(\frac{mv_0^2}{k_B}\right)\frac{dT^\star}{ds}\frac{ds}{dx} \\ = -\frac{15}{4}\frac{k_B\eta}{m}\left(\frac{mv_0^2}{k_B}\right)\frac{dT^\star}{ds}\frac{ds}{dx}$$

or

$$\frac{9\eta^\star}{4}\frac{v^{\star2}}{T^\star}\left(v^\star - (1+T_0^\star)\right)\frac{dv^\star}{ds} + \frac{9\eta^\star}{8}\left(5 - 3\frac{v^{\star2}}{T^\star}\right)\frac{dT^\star}{ds} + v^{\star2} - 2(1+T_0^\star)v^\star - 3T^\star + 5T_0^\star + 1 = 0, \tag{13b}$$

where we have used Eqs. (9).

Equations (13a) and (13b) can be used to obtain the following explicit dynamical system,

$$\frac{dv^\star}{ds} = \frac{4T^\star p_1(v^\star,T^\star,T_0^\star)}{3\eta^\star v^\star q(v^\star,T^\star,T_0^\star)}, \tag{14a}$$

$$\frac{dT^\star}{ds} = \frac{8T^\star p_2(v^\star,T^\star,T_0^\star)}{9\eta^\star q(v^\star,T^\star,T_0^\star)}, \tag{14b}$$

with

$$p_1(v^\star,T^\star,T_0^\star) = 11v^{\star 4} - 13(1+T_0^\star)v^{\star 3} + (2 - 12T^\star + 10T_0^\star)v^{\star 2} + 15T^\star(1+T_0^\star)v^\star - 15T^{\star 2}, \tag{15a}$$

$$p_2(v^\star,T^\star,T_0^\star) = 6v^{\star 4} - 12(1+T_0^\star)v^{\star 3} + \left(6 + 25T^\star + 9T_0^{\star 2} + 3T_0^\star\right)v^{\star 2} - 23T^\star(1+T_0^\star)v^\star - [21T^{\star 2} - 7T^\star(1+5T_0^\star)], \tag{15b}$$

and

$$q(v^\star,T^\star,T_0^\star) = -15v^{\star 4} + 6(1+T_0^\star)v^{\star 3} + 36T^\star v^{\star 2} - 35T^{\star 2}. \tag{15c}$$

For the Navier-Stokes equations the constitutive equations are obtained from Eqs. (7a) and (7b) by taking the relaxation times equal to zero. Substitution of the resulting fluxes into the equations of conservation of momentum and energy [see Eqs. (4b) and (4c)] gives the following reduced form of them,

$$\frac{dv^\star}{ds} = \frac{v^{\star 2} - (T_0^\star + 1)v^\star + T^\star}{v^\star \eta^\star}, \tag{16a}$$

$$\frac{dT^\star}{ds} = \frac{2k_B\eta_0}{3m\kappa_0}\frac{-v^{\star 2} + 2(1+T_0^\star)v^\star + 3T^\star - (5T_0^\star+1)}{\kappa^\star}. \tag{16b}$$

In this case we decided not to use only the first Sonine approximation, in order to see what are the differences between assuming and not assuming this approximation; they are expected to be small according to the analysis on the deviations of the experimental data for the transport coefficients given in Sec. III. This is actually the case.

The reduced form of the fluxes can be obtained from Eqs. (9), (11a), and (11b):

$$\sigma^\star \equiv \frac{\sigma}{\rho_0 u_0^2} = \frac{T^\star}{v^\star} + v^\star - (1+T_0^\star), \tag{17a}$$

$$Q^\star \equiv \frac{Q}{\rho_0 u_0^3} = \frac{v^{\star 2}}{2} - (1+T_0^\star)v^\star - \frac{3}{2}T^\star + \frac{5T_0^\star+1}{2} = 2v^{\star 2} - \frac{3}{2}\sigma^\star v^\star - \frac{5}{2}(1+T_0^\star)v^\star + \frac{5}{2}T_0^\star + \frac{1}{2}. \tag{17b}$$

These expressions do not depend on the constitutive equations and are therefore of a general character.

Notice that if we express $T^\star$ as a function of $v^\star$ we would have to solve

$$\frac{dT^\star}{dv^\star} = \frac{2}{3}\frac{v^\star p_2(v^\star,T^\star(v^\star),T_0^\star)}{p_1(v^\star,T^\star(v^\star),T_0^\star)}, \tag{18}$$

which is independent of the viscosity, and conclude that locally the solution curves of the dynamical system are independent of the viscosity (independent of the interaction potential). One can use constant transport coefficients, for example (but related according to the first Sonine approximation), and the solution curves should be the same as when the viscosity is proportional to the temperature, as happens for the Maxwell interaction model. Also, the result can be generalized when the first Sonine approximation does not hold, provided that the temperature dependence of the viscosity and thermal conductivity be the same. The same result is known to hold for the Navier-Stokes equations [6,12] and can be easily verified.

The solution to the Maxwell-Cattaneo dynamical system [Eqs. (14)] that we are seeking, corresponding to the shock wave, must asymptotically tend to the Rankine-Hugoniot jump conditions, that in reduced variables are given by

$$v_0^\star = 1, \quad T_0^\star = T_0^\star, \quad v_1^\star = \tfrac{5}{4}T_0^\star + \tfrac{1}{4}, \quad T_1^\star = \tfrac{7}{8}T_0^\star + \tfrac{3}{16} - \tfrac{5}{16}T_0^{\star 2}. \tag{19}$$

Subscripts 0 and 1 refer to the cold part of the shock (also called upflow or upstream) and hot part of the shock (also called downflow or downstream), respectively. For $T_0^\star = 3/5$ there is no compression; a twofold compression corresponds to $T_0^\star = 1/5$ ($\rho_1 = 2\rho_0$); the maximum compression attainable for a dilute monoatomic gas is fourfold, corresponding to $T_0^\star = 0$ ($\rho_1 = 4\rho_0$).

In general terms the problem that we are trying to solve corresponds to finding a specific solution to the differential equation $\mathbf{y}'(s) = \mathbf{F}(\mathbf{y}(s),\boldsymbol{\omega})$, where $\mathbf{F} : A \subset \mathbb{R}^n \times \mathbb{R}^k \to \mathbb{R}^n$ is a vector field on $\mathbb{R}^n$ that depends on k parameters represented by $\boldsymbol{\omega}$, and $\mathbf{y} : (a,b) \to \mathbb{R}^n$ is a differentiable function, where $\mathbf{y}'(s)$ denotes the derivative of the function $\mathbf{y}$ at the point $s \in (a,b)$. In the literature one can find cases for which $n = 2$ and $k = 1$ [20], $n = 3$ and $k = 1$ (Brenner's two-velocity hydrodynamics [38,43,62], Bobylev's generalized Burnett equations [41]), $n = 4$ and $k = 1$ (13-moment equations [12], regularized 13-moment equations [21], Burnett [31,32]). For examples of higher dimension dynamical systems such as the super-Burnett, the augmented Burnett equations, and their variants, see [25,28,33]; for theories that include more moments than Grad's 13-moment approximation, see [18]; for

regularizations of the Burnett equations, see [34]. The two dynamical systems considered here, the Maxwell-Cattaneo and Navier-Stokes dynamical systems, correspond to $n = 2$ and $k = 1$, and the specific solution sought should tend asymptotically to the critical points given by the Rankine-Hugoniot conditions; see Eq. (19). In the mathematical literature a critical point, $\mathbf{y}^\star$, is defined by the condition $\mathbf{F}(\mathbf{y}^\star,\boldsymbol{\omega}) = 0$; the Rankine-Hugoniot jump conditions provide two critical points for the dynamical systems here considered; they are also identified with two equilibrium points of thermodynamics. The specific solution curve (orbit) that asymptotically tends to the two equilibrium points given by the Rankine-Hugoniot jump conditions is named a heteroclinic trajectory—or *orbit* in the mathematical literature.

III. SHOCK WAVE STRUCTURE

In this section we consider a specific case that we can compare with experimental information. We choose argon at standard conditions according to the definition by the National Institute of Standards and Technology: a temperature of $T_0 = 293.15$ K (20 °C) and a pressure of $p = 101.325$ kPa (one atmosphere), to represent upstream. We need to know also the viscosity and thermal conductivity at T_0, and we use the values provided by the corresponding state principle (CSP) [70] that gives

$$\eta_0 = 22.39\ \mu\text{Pa s}, \quad \kappa_0 = 17.49\ \frac{\text{mW}}{\text{m K}}. \tag{20}$$

Using these values we obtain that $k_B\eta_0/m\kappa_0 \approx 0.266491$, which differs from 4/15 by about 0.08%; see Eq. (6). For the whole range of temperatures (50 to 3000 K) the tabulated values of the CSP give that $k_B\eta/m\kappa$ deviates from 4/15 by less than 0.4%, so that the first Sonine approximation is good. Also, the reduced viscosity and thermal conductivity, $\eta^\star = \eta/\eta_0$ and $\kappa^\star = \kappa/\kappa_0$, differ at most by about 0.3% so that the assumption of the same temperature dependence of both transport coefficients is also good. The CSP is also used to provide the temperature behavior of both transport coefficients; the estimated accuracy of the correlation is 0.3% for the viscosity and 0.7% for the thermal conductivity in the temperature range from 50 to 1000 K, a range that is enough for us since the Mach numbers considered will be from 1 to 2 for reasons that will be clear below. Actually, the highest temperature considered by the correlation is 3000 K so that the largest Mach number is a little less than 4.5. Higher Mach numbers can also be considered, as is standardly done, by assuming a power law temperature dependence of the viscosity of the form $\eta \sim T^\gamma$ (which we refer to as the soft sphere model since such temperature dependence of the viscosity is obtained assuming an interaction potential of the form $\sim r^{-\nu}$, with r the interatomic distance [10]), and fitting the value of γ to the experimental data [38]. We can calculate the values of the relaxation times given by Eq. (6) using the values of the transport coefficients given by the CSP [see Eq. (20)], and the ideal equation of state. The values at upflow are

$$\tau_\sigma \approx 2.21 \times 10^{-10}\ \text{s}, \quad \tau_Q \approx 3.32 \times 10^{-10}\ \text{s}. \tag{21}$$

For a 2.3-fold compression shock wave ($M = 2$) the values of the velocity, pressure, temperature, transport coefficients, and relaxation times at downflow are

$$\begin{aligned} &v_1 = 279.0\ \frac{\text{m}}{\text{s}}, \quad p_1 = 481.3\ \text{kPa}, \quad T_1 = 609.2\ \text{K}, \\ &\eta_1 = 39.48\ \mu\text{Pa s}, \quad \kappa_1 = 30.89\ \frac{\text{mW}}{\text{m K}}, \\ &\tau_\sigma = 0.82 \times 10^{-10}\ \text{s}, \quad \tau_Q = 1.23 \times 10^{-10}\ \text{s}. \end{aligned} \tag{22}$$

Here we assume that upflow is at standard conditions ($v_0 = 637.8$ m/s) and use the Rankine-Hugoniot jump conditions to evaluate the pressure, velocity, and temperature at downflow.

There are several implementations of the direct simulation Monte Carlo method (DSMC), such as dsmcFoam [71], but we will follow the one by Bird [29]. He considers two interaction models—the variable hard sphere (VHS) model and the variable soft sphere model (VSS)—to study shock waves in argon. The VSS model is characterized by the viscosity temperature index (γ) and a parameter α (exponent in the VSS molecular models); see [29] for the details. According to Bird realistic values for them are $\gamma = 3/4$ and $\alpha = 1.5325$. Bird reduces the distance with his mean-free path (λ_B) given by

$$\lambda_B = \frac{4\alpha(5-2\gamma)(7-2\gamma)}{5\sqrt{\pi}(\alpha+1)(\alpha+2)}\frac{\beta_0\eta_0}{\rho_0}, \quad \text{where } \beta_0 = \sqrt{\frac{m}{2k_BT_0}}. \tag{23}$$

Alsmeyer gives experimental information for shock waves in argon [72]. He gives the normalized density profiles (ρ_n)

$$\rho_n \equiv \frac{\rho - \rho_0}{\rho_1 - \rho_0} \tag{24}$$

as a function of the reduced distance $s_A \equiv x/\lambda_A$ where λ_A is his mean-free path,

$$\lambda_A = \frac{16}{5}\left(\frac{5}{3}\frac{1}{2\pi}\right)^{1/2}\frac{\eta_0}{\rho_0 a_0}, \quad \text{with } a_0 = \sqrt{\frac{5}{3}\frac{k_BT_0}{m}}, \tag{25}$$

the sound velocity. The relation between the three different lengths used to reduce the distance with an upflow temperature T_0 is the following,

$$\lambda_A = \frac{4(\alpha+1)(\alpha+2)}{\alpha(5-2\gamma)(7-2\gamma)}\lambda_B, \quad \lambda = \frac{5}{12}\sqrt{2\pi T_0^\star}\lambda_A. \tag{26}$$

Alsmeyer evaluated his mean-free path at upstream, which he calls the front of the shock wave. At $T_0 = 300$ K and $p_0 = 50$ mTorr (we have changed his notation to conform with ours) he reports the value $\lambda_A = 1.098$ mm for argon. Using the CSP to evaluate the viscosity we obtain $\lambda_A = 1.093$ mm for argon at the same conditions.

There is a useful sensitive property, called the density asymmetry quotient [38] or asymmetry of the density profiles [72,73] (Q_ρ); it can be calculated from measurements, and is given by

$$Q_\rho = \frac{\int_{-\infty}^0 \rho_n(s)ds}{\int_0^\infty (1-\rho_n(s))ds}, \tag{27}$$

and will be considered in our comparisons with the experimental information; $s = 0$ corresponds to the value at which

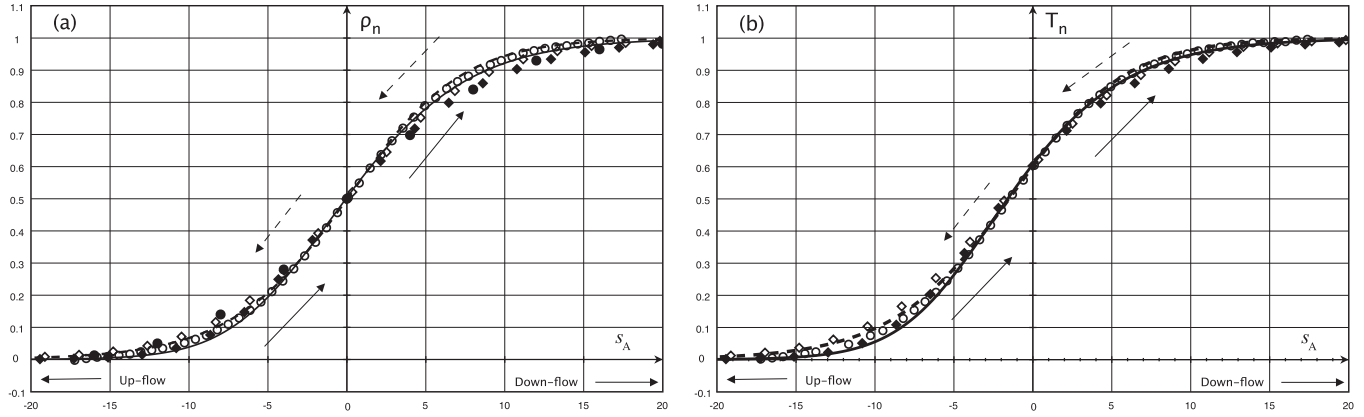

FIG. 1. (a) Normalized density vs reduced distance, ρ_n vs $s_A = x/\lambda_A$, for argon at $M = 1.2$. (b) Normalized temperature vs reduced distance, T_n vs $s_A = x/\lambda_A$, for argon at $M = 1.2$. Solid line: Maxwell-Cattaneo with the CSP; dashed line: Navier-Stokes equations with the CSP; solid circles: experimental values by Garen *et al.* [74]; circles: DSMC; solid diamonds: Maxwell-Cattaneo for $\gamma = 2$; open diamonds: Navier-Stokes for $\gamma = 2$. The solid arrows for $\rho_n > 0$ indicate the sense in which the integration for the Maxwell-Cattaneo equations is performed (+) while the dashed lines indicate the sense of integration for the Navier-Stokes equations (−).

$\rho_n = 1/2$. Other normalized profiles of interest are those corresponding to velocity and temperature defined by

$$u_n \equiv \frac{u - u_0}{u_1 - u_0}, \quad T_n \equiv \frac{T - T_0}{T_1 - T_0}. \tag{28}$$

There is not experimental information for the normalized temperature profile so that the comparisons are done with DSMC.

In the following, we will use Adams' method, as implemented by the Numerical Algorithms Group (NAG), to solve the dynamical systems given by Eqs. (14), (16), and (18). We use a tolerance (accuracy goal) for Adams' method of value 10^{-15}, unless stated otherwise. A discussion of the method when solving the Navier-Stokes equations for the shock wave problem, and its comparisons with a couple of versions of the Runge-Kutta method and the backward differentiation formula, is available [75].

A. Mach numbers near 1

In Fig. 1 we provide the normalized density and temperature profiles for $M = 1.2$; they are obtained by solving the two sets of differential equations: the Maxwell-Cattaneo case, Eqs. (14), and those corresponding to the Navier-Stokes equations, Eqs. (16). Also included are the experimental values by Garen *et al.* [74] for argon at $M = 1.2$. We found good agreement with the results for the Navier-Stokes equations at $M = 1.2$ reported by Garen *et al.* for the hard sphere model ($\gamma = 1/2$).

The initial conditions used to obtain the profiles, as well as the sense in which the integration is performed (see below), are given in Table I. They are determined by requiring the normalized density profile at $s = 0$ (or $s_A = 0$) to have the value $1/2$; this definition makes sense if there are not two values of s, say $s_1 \neq s_2$, for which $\rho_n(s_1) = \rho_n(s_2) = 1/2$; in particular for monotonic profiles the origin is well defined. If the integration is performed by increasing the reduced distance s, we say that the integration is carried out in the positive sense (+), and similarly, if the integration is done by decreasing s, we say that it is performed in the negative sense (−). For the Navier-Stokes, upflow is an unstable node (there is a neighborhood around it such that any solution curve with an initial condition in the neighborhood goes away from the critical point [76]), and downflow is a saddle (for initial conditions near the critical point some solution curves tend to downflow while others go away from the critical point), and for the Maxwell-Cattaneo equations upflow is a saddle and downflow is a stable node (there is a neighborhood around it such that any solution curve with an initial condition in the neighborhood tends to the critical point). The nature of the

TABLE I. Initial conditions for the Maxwell-Cattaneo (MC) and the Navier-Stokes (NS) dynamical systems using the corresponding states principle (CSP) and the soft sphere model characterized by γ. Figures in the decimal representation of some numbers were rounded off.

M	$T_0^\star$	$v_1^\star$	$T_1^\star$	System	Model	Sense	s_0	$v^\star(s_0)$	$T^\star(s_0)$
1.2	5/12	37/48	1147/2304	MC	CSP	+	−115.2664	$1 - 10^{-14}$	$T_0^\star$
					$\gamma = 2$	+	−83.2585	$1 - 10^{-10}$	
				NS	CSP	−	74.3799	$v_1^\star + 10^{-10}$	
					$\gamma = 2$	−	164.2455	$v_1^\star + 10^{-12}$	
1.55	240/961	0.562175	0.386532	NS	CSP	−	43.0137	$v_1^\star + 10^{-14}$	
					$\gamma = 1/2$	−	28.7783	$v_1^\star + 10^{-14}$	
2.0	3/20	7/16	399/1280	MC	CSP	+	−26.1277	$v_1^\star + 10^{-14}$	
				NS	CSP	−	15.7572	$v_1^\star + 10^{-10}$	

TABLE II. Nature of the critical points and existence of a numerical shock wave solution for the Maxwell-Cattaneo dynamical system as a function of the Mach number. The numerical shock wave solutions for $M \in (1, M_1)$, $M_1 \approx 1.2716$, are in good agreement with experiments (when available) and simulations. For $M \in (M_1, M_2)$, $M_2 \approx 1.90$, there are no numerical shock wave solutions. For $M \in (M_2, M_3)$, $M_3 = 2.5$, there are numerical shock wave solutions that differ widely from experiments and simulations. We have not explored the case $M > 2.5$ since for $M \in [1.90, 2.5]$ the numerical solutions are "unphysical." The nature of the critical points is independent of the viscosity and the thermal conductivity; see discussion after Eq. (18).

Mach Number	Nature of the critical points	Standard numerical shock wave solution?
$1 < M < M_1 \approx 1.2716$	Upflow is a saddle Downflow is a stable node	Yes
$M_1 < M < M_2^c \approx 1.4657$	Both critical points are saddles	No
$M_2^c < M < M_2 \approx 1.90$	Upflow is a stable node Downflow is a saddle	No
$M_2 < M < M_3 = 2.5$		Yes

critical points determines the sense in which the integration must be carried out, and it can be determined by analyzing the eigenvalues of the Jacobian matrix of the vector field defined by a given set of differential equations at each critical point [76].

The nature of the critical points for the Maxwell-Cattaneo dynamical system for $M \in (1, \infty)$ is given in Table II. From Fig. 1 ($M = 1.2$) we notice that the profiles obtained using the CSP are similar for the Navier-Stokes and the Maxwell-Cattaneo equations; for $s_A > 0$ the latter equations give better agreement with the experimental data than the former equations, but the opposite is observed for $s_A < 0$. The same happens for the unrealistic soft sphere model with $\gamma = 2$ shown in Fig. 1. To see why this model is unrealistic, notice that if the viscosity at upflow is given by the CSP, then assuming $\eta \sim T^2$ we will have that the viscosity at $T = 423.15$ K (the temperature at downflow is approximately 400 K for $M = 1.25$) is 39.25 μPa s, that is higher than the CSP value, $\eta_{CSP} = 30.11$ μPa s, by about 17%. At $T = 1273.15$ K the viscosity evaluated using $\gamma = 2$ is about five times the value given by the CSP.

The reduced stress and heat flux are given in Fig. 2: the qualitative features of the reduced fluxes corresponding to the Navier-Stokes and the Maxwell-Cattaneo equations are similar. The quantitative differences that can be observed in the figure reflect the differences of the corresponding normalized density profiles. Therefore, neither the normalized profiles nor the reduced fluxes provide a clear-cut preference between NS or MC for the particular Mach number considered so far: $M = 1.2$. Another test is to consider the asymmetry quotient given by Eq. (27). It is especially useful for weak shocks (Mach numbers near one) since it is known [26,38,72] that experiments give a value of Q_ρ less than 1 for Mach numbers less than 2.5 while the Navier-Stokes equations give a value greater than 1. At $M = 2.5$ the difference between experiments and the Navier-Stokes equations can be 35% [72]. For $M = 1.2$ with $\gamma = 0.72$ the Navier-Stokes equations give $Q_\rho = 1.07$, which is in good agreement with previous works [38], while the Maxwell-Cattaneo equations with the same γ give $Q_\rho = 0.822$; experiments give a value of about 0.93. The well known explicit solution to the Navier-Stokes equations in terms of a hyperbolic tangent function given by Landau [2] for constant transport coefficients and weak shocks gives $Q_\rho = 1.0$.

As we will now show, the superiority of Navier-Stokes equations as a physical theory with respect to the

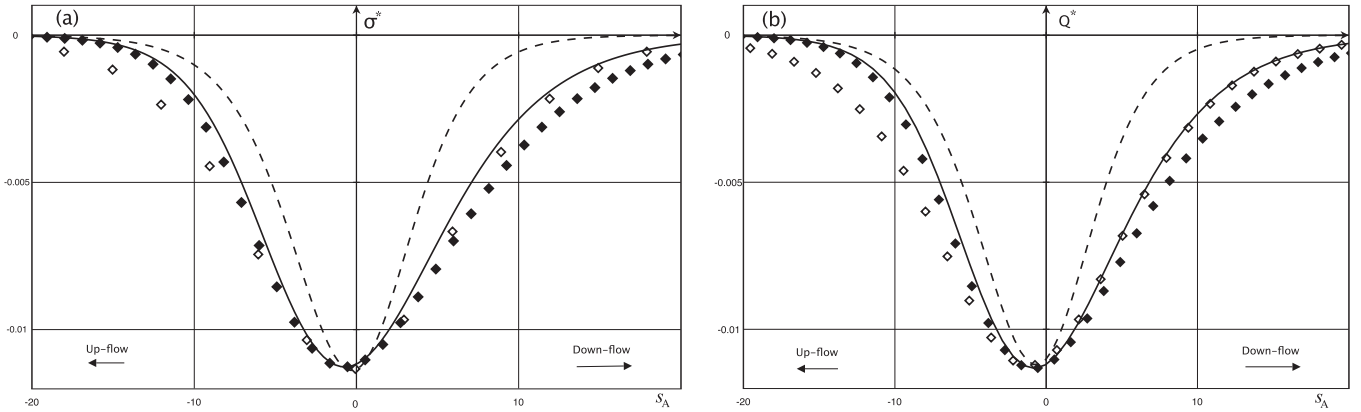

FIG. 2. (a) Reduced stress tensor vs reduced distance, $\sigma^\star$ vs $s_A = x/\lambda_A$, for argon at $M = 1.2$. (b) Reduced heat flux vs reduced distance, $Q^\star$ vs $s_A = x/\lambda_A$, for argon at $M = 1.2$. Solid line: Maxwell-Cattaneo with the CSP; dashed line: Navier-Stokes equations with the CSP; solid diamonds: Maxwell-Cattaneo for $\gamma = 2$; open diamonds: Navier-Stokes for $\gamma = 2$.

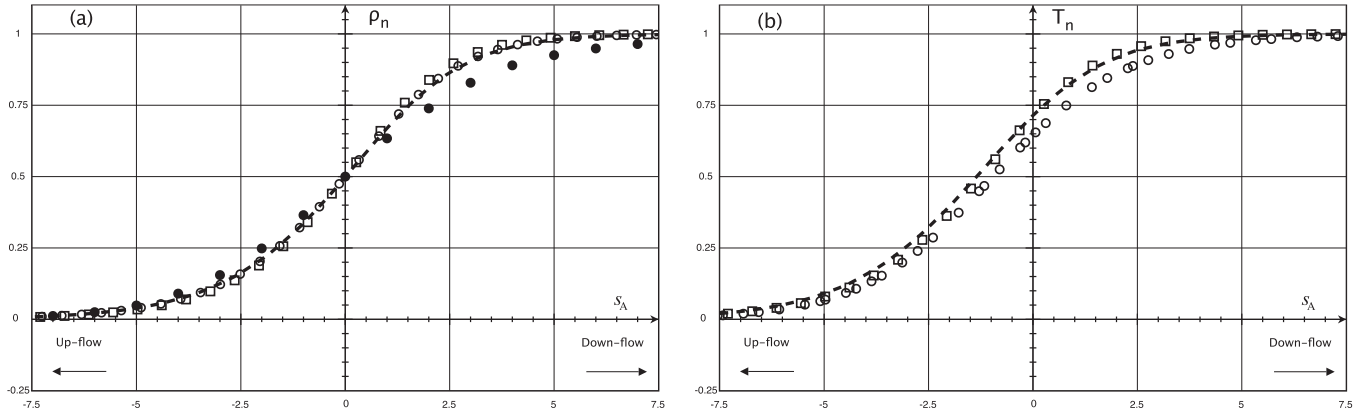

FIG. 3. (a) Normalized density vs reduced distance, ρ_n vs s_A, for argon at $M = 1.55$. (b) Normalized temperature vs reduced distance, T_n vs s_A, for argon at $M = 1.55$. Dashed line: Navier-Stokes with the CSP; open circles: DSMC with $\gamma = 0.72$ and $\alpha = 1$; solid circles: experimental values by Alsmeyer [72]; open squares: Navier-Stokes for the hard sphere model ($\gamma = 1/2$).

Maxwell-Cattaneo equations becomes evident as we increase the Mach number.

B. On the possible lack of "standard" shock wave solutions to the Maxwell-Cattaneo equations

In Fig. 3 we give the normalized density and temperature profiles for $M = 1.55$ but we do not provide the Maxwell-Cattaneo profiles since we have been unable to find what we consider to be standard numerical shock wave solutions. The important point to be cleared up is whether shock wave solutions exist or not in this case. The possibility of lack of standard shock wave solutions for the Maxwell-Cattaneo dynamical system is not surprising since, as we mentioned above, there are several moment methods that do not have shock wave solutions above a certain Mach number [12,15–19].

In Fig. 4(a) we provide the shape of the normalized density profiles obtained with the Maxwell-Cattaneo equations as the Mach number is increased; in particular for $M = 1.35$, only part of the profile can be obtained with a tolerance (accuracy goal) of value 10^{-15}; the numerical reason is a floating division by zero detected by the NAG Fortran compiler, which we attribute to q becoming very small in Eqs. (14). The shape of such solution, in the $v^\star$-$T^\star$ plane, is given in Fig. 5(a). For greater values of the tolerance, such as 10^{-13}, we can continue the solution, as shown in Fig. 4(b), and again we reach the conclusion that such a solution does not represent a shock wave solution (similar results for Grad's 13-moment equations have been reported in the literature [21]). In the $v^\star$-$T^\star$ plane it crosses the loci of points given by $q(v^\star, T^\star, T_0^\star) = 0$ and continues to the origin, without reaching downflow, of the $v^\star$-$T^\star$ plane. In Fig. 4(b) we also show a solution to the Maxwell-Cattaneo that starts near downflow; we have separated the two numerical solutions on purpose so that they can be discerned. If the two points at which the spikes appear are brought together, these spikes merge and we are led with two curves: one of them consists in the spikes merged, and the other is near the DSMC data, specially at downflow; we do not consider this as a "standard" shock wave solution because the parts of the resulting curve run in different directions, but perhaps there could be another theoretical context, such as weak solutions, in which such behavior is allowed. For us, the results give evidence that no "standard" shock wave

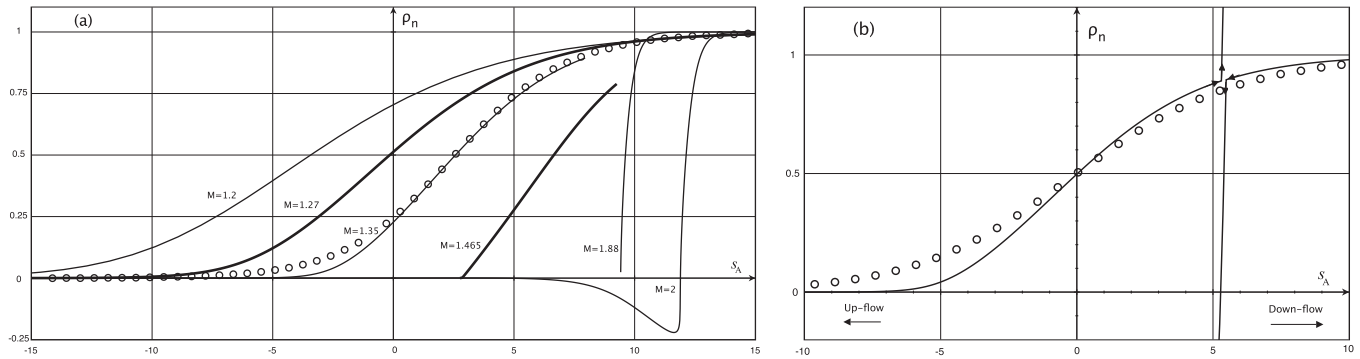

FIG. 4. (a) Normalized density profiles as a function of the reduced distance for different Mach numbers: ρ_n vs s_A, and a tolerance of value 10^{-15}. For convenience, we relax the condition that the normalized density profiles have the value $1/2$ at $s = 0$. Solid lines: Maxwell-Cattaneo equations: for each curve upflow is at the left, and downflow at the right; open circles: DSMC for $M = 1.35$. For $M = 1.88{,}2$, the solutions are such that their corresponding orbits are outside of the loci of singularities; for the other Mach numbers their corresponding orbits are inside. (b) Normalized density profiles as a function of the reduced distance for different Mach numbers, ρ_n vs s_A for $M = 1.35$, and a tolerance of value 10^{-13}. Solid lines: Maxwell-Cattaneo equations; open circles: DSMC for $M = 1.35$.

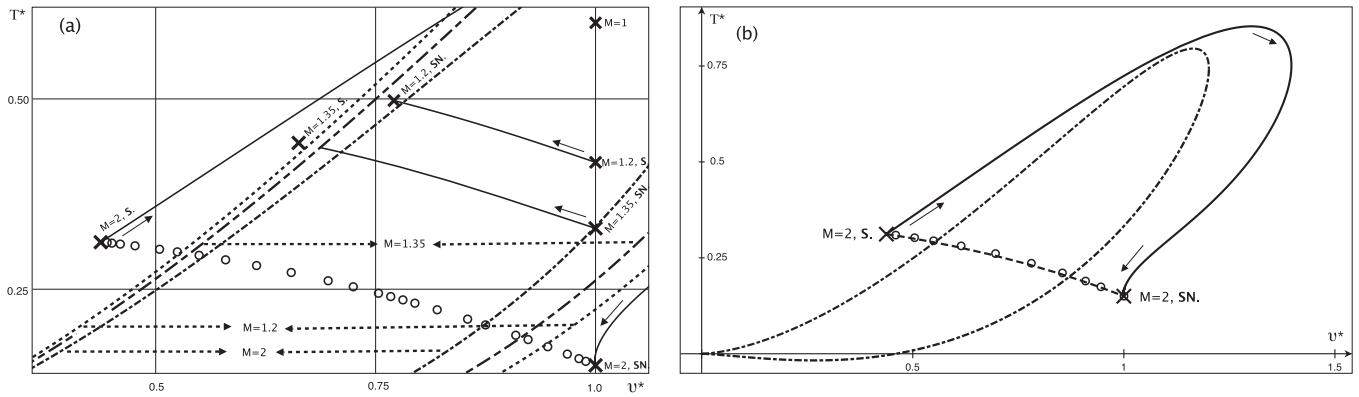

FIG. 5. (a) Orbits and loci of singularities [$q = 0$; see (15c)] in the $T^\star$-$v^\star$ plane for different Mach numbers. Solid lines: solution curves for the Maxwell-Cattaneo equations using the CSP; open circles: DSMC with $\gamma = 0.81$ and $\alpha^{-1} = 0.6525$ for $M = 2$; crosses: equilibrium points; dotted line: loci of singularities ($q = 0$) for the Maxwell-Cattaneo equations for $M = 1.2$; long-dash–dashed line: loci of singularities for the Maxwell-Cattaneo equations for $M \approx 1.35$; dot-dashed line: loci of singularities for the Maxwell-Cattaneo equations for $M = 2$. (b) Orbits and loci of singularities [$q = 0$; see (15c)] in the $T^\star$-$v^\star$ plane for $M = 2$. Solid lines: solution curves for the Maxwell-Cattaneo equations using the CSP; open circles: DSMC with $\gamma = 0.81$ and $\alpha^{-1} = 0.6525$ for $M = 2$; crosses: equilibrium points for $M = 2$; dot-dashed line: loci of singularities ($q = 0$) for the Maxwell-Cattaneo equations for $M = 2$; dashed line: Navier-Stokes using the CSP. The nature of each critical point for the Maxwell-Cattaneo equations shown in the graph is given by the following code: S ≡ saddle, SN ≡ stable node.

numerical solutions exist, though the nonstandard construction described may be used to study a more general theoretical framework, after all; there is agreement with the DSMC simulations.

However, not all the partial solutions that can be calculated have the form of a typical shock wave solution; in Fig. 4 the piece of the profile calculated for $M = 1.465$ does not have the form of a typical shock wave since now the derivative near upflow of the normalized density profile is too steep. Also, the piece of the profile for $M = 1.88$ shows a huge derivative; this is a result of that it is near the loci of singularities, and in this case its manifestation is a very narrow profile so that the manifestations of singularities are narrow profiles. It should be pointed out that the orbit for $M = 1.465$ is inside the corresponding loci of singularities, while that for $M = 1.88$ is outside.

There is a simple geometrical argument that reveals what are some of the problems that we face in order to obtain a shock wave solution in some cases. In the following it will be convenient to notice that even for $v^\star \neq 0$ the loci of singularities of the vector field [denoted by $L_{\mathbf{F}}$; see Eq. (14)] may differ from the loci of points defined by the condition $q(v^\star, T^\star, T_0^\star) = 0$ (denoted by L_q), since the loci of points given by $p_1(v^\star, T^\star, T_0^\star) = 0$ and $p_2(v^\star, T^\star, T_0^\star) = 0$ (denoted by L_{p_1} and L_{p_2}, respectively) can intersect L_q. In Fig. 5(a) we provide the critical points for three Mach numbers, and part of the loci of the singularities for the Maxwell-Cattaneo differential equations. For the Mach numbers considered, L_q has the shape shown by the dot-dashed line shown in Fig. 5(b); it is a simple closed curve (a Jordan curve) that divides $\mathbb{R}^2$ in two regions: the exterior—an unbounded region—and the interior—a bounded region [77]. When $1 \leqslant M < M_1^c$—M_1^c will be determined below—the two critical points are inside, and a heteroclinic solution curve can exist. As the Mach number is increased from 1, downflow eventually intersects L_q, the Mach number (or the value of $T_0^\star$) at which the intersection occurs can be obtained solving the equation; see Eqs. (15c) and (19):

$$0 = q((1 + T_0^\star)/4, \left(-5\, T_0^{\star 2} + 14\, T_0^\star + 3\right)/16, T_0^\star)$$
$$= -\tfrac{1}{128}\left(235\, T_0^{\star 2} - 354\, T_0^{\star 2} + 99\right)\left(1 + 5\, T_0^{\star 2}\right)^2. \quad (29)$$

The two roots $T_0^\star = -1/5$ are unphysical because T is the absolute temperature, and from the other two roots we keep $T_0^\star = (177 - 24\sqrt{14})/235 \approx 0.3711$ ($M_1^c \approx 1.2716$) since the other root gives a "Mach" number outside the range of our interest: $M \in [1, \infty)$.

When $M_1 < M < M_2^c$—where M_2^c can be determined by requiring that upflow intersect L_q leading to $T_0^\star = 3(1 - \sqrt{14}/7)/5 \approx 0.2793$ or $M_2^c \approx 1.4657$—one critical point (upflow) is in the interior of L_q and the other one (downflow) is in the exterior, so that any curve joining the two critical points must necessarily intersect L_q. In particular, if there is a solution to the Maxwell-Cattaneo equations that joins the critical points, it must intersect L_q, meaning that the derivatives may be infinite; this would contradict the existence of a heteroclinic orbit that must have smooth derivatives, if we leave out weak solutions. Our computations (see Fig. 5) for $M = 1.35$ with a tolerance of value 10^{-15} show that the numerical solution curve cannot cross L_q but that it crosses L_q for a tolerance of value 10^{-13}; this just reflects that tight accuracy requirements lead to a conservative integration scheme in which the next move is not allowed; in other words, tight accuracy eliminates the spikes in this case. If the one-dimensional system given by Eq. (18) is solved with a tolerance of value 10^{-15} and with the same initial condition as the two-dimensional Maxwell-Cattaneo system ($v^\star = 0.99999999999999$, $T^\star = 0.33$), the resulting orbit is practically the same as the one obtained using the two-dimensional Maxwell-Cattaneo system with a tolerance of value 10^{-13}; this suggests favoring the lower accuracy goal result. However, the argument is not conclusive because the point at which the numerical solutions bend (the spikes appear) corresponds to a singular point for the one-dimensional system. We favor the tight accuracy result.

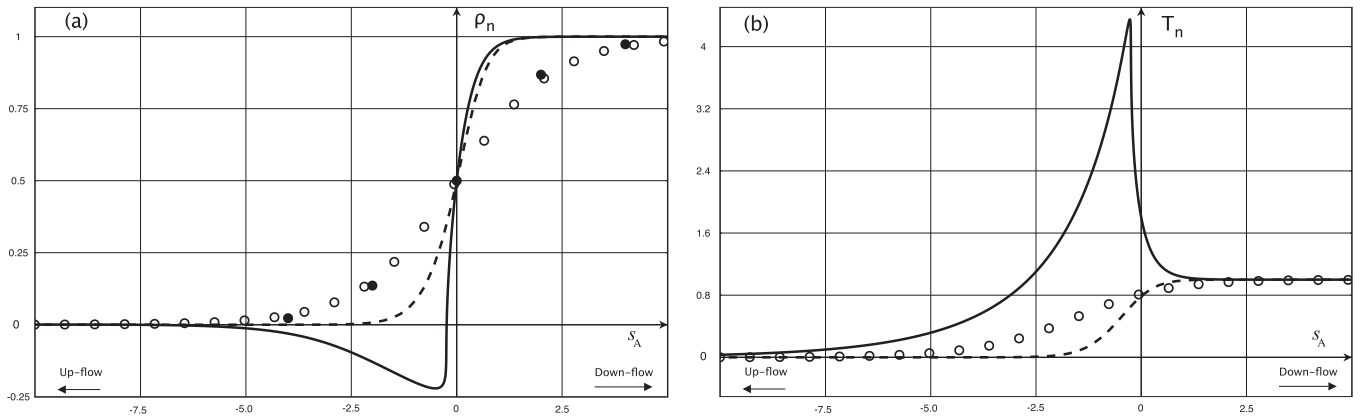

FIG. 6. (a) Normalized density profile vs reduced distance, ρ_n vs $s_A = x/\lambda_A$, for argon at $M = 2$. (b) Normalized temperature profile vs reduced distance, T_n vs $s_A = x/\lambda_A$, for argon at $M = 2$. Solid line: Maxwell-Cattaneo with the CSP; dashed line: Navier-Stokes equations with the CSP; solid circles: experimental values by Alsmeyer [72] for $M = 2.05$; open circles: DSMC for $\gamma = 0.81$ and $\alpha^{-1} = 0.6525$.

The argument just given makes plausible that a heteroclinic connection may not be possible when the critical points are in the different regions (the interior and exterior) of the loci of singularities, and this happens for $M \in (M_1^c, M_2^c)$ or $1.2716 \lessapprox M \lessapprox 1.4657$. However, in our case we did not find a numerical shock wave solution for $M = 1.55$ that is outside the previous range of Mach numbers and therefore the two critical points are in the exterior to the loci of singularities. In this case we think that no solution is possible due to the proximity of one of the critical points to the singularity curve. We have been unable to find standard numerical shock wave solutions to the Maxwell-Cattaneo system for Mach numbers lower than (approximately) $M_2 = 1.9$.

C. "Unphysical" shock wave solutions to the Maxwell-Cattaneo equations

Apart from the lack of numerical solutions discussed in the previous section, it turns out that as the Mach number is increased to the value $M = 2$, corresponding to a 2.3-fold compression, we have been able to find a numerical shock wave solution to the Maxwell-Cattaneo dynamical system; see Fig. 5. There is however a subtle issue that needs to be cleared up in our numerical solution for $M = 2$: since the solution curve to the Maxwell-Cattaneo equations must go from downflow to upflow, upflow cannot be at the left of downflow when considering the profiles, as is the case for the profiles in Figs. 1–3, because it is a stable node. For the Navier-Stokes equations upflow is always an unstable node while downflow is a saddle; in this case upflow must always be at the left of downflow.

There are two ways of solving the subtle point mentioned above to make a comparison. The first is to obtain the profile for the Maxwell-Cattaneo equations for $M > M_2^c$ (we take $M = 2$ corresponding to a 2.3-fold compression) in which upflow is at the right of downflow and make the transformation $s_A \to -s_A$. The second is to compare the orbits as we have done; each way has its own advantages and disadvantages; so, we have provided both: in Fig. 5 we provide the orbits, and in Figs. 6 and 7 the profiles. Figure 6 shows that the Maxwell-Cattaneo equations considered in this work fail at $M = 2$ when compared with the experimental data; comparisons with DSMC and the Navier-Equations are also shown. The last ones give narrower profiles than the experiment, but are certainly

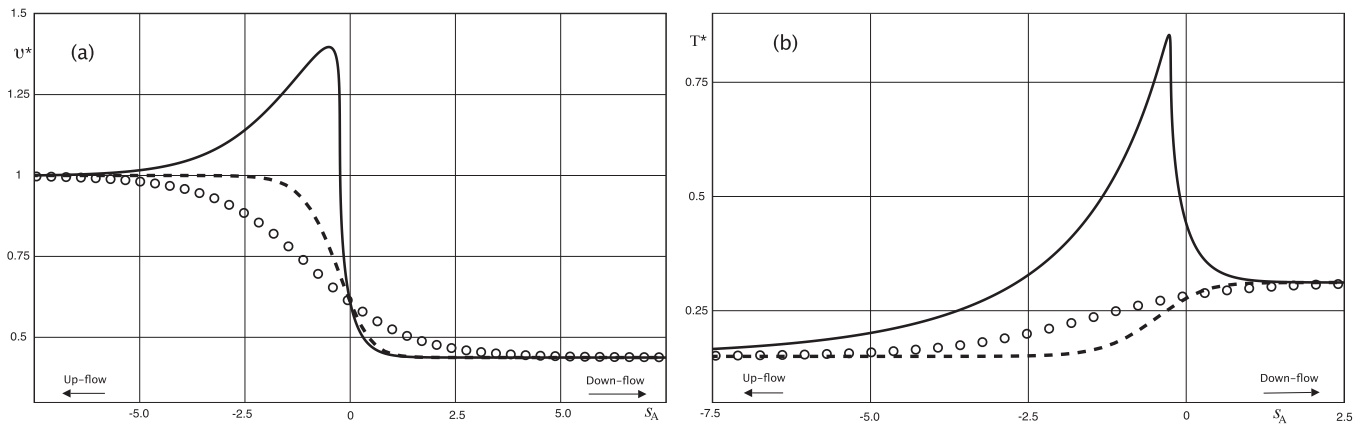

FIG. 7. (a) Reduced velocity profile vs reduced distance, $v^\star$ vs s_A, $s_A = x/\lambda_A$, for argon at $M = 2$. (b) Reduced temperature profile vs reduced distance, $v^\star$ vs s_A, $s_A = x/\lambda_A$, for argon at $M = 2$. Solid line: Maxwell-Cattaneo with the CSP; dashed line: Navier-Stokes equations with the CSP; open circles: DSMC for $\gamma = 0.81$ and $\alpha^{-1} = 0.6525$. In order to compare with the Navier-Stokes equations and DSMC, the transformation $s_A \to -s_A$ was used for the solutions of the Maxwell-Cattaneo dynamical system.

better than the Maxwell-Cattaneo equations for $M = 2$. From Figs. 6 and 7 it is clear that the profiles are nonmonotonic.

An important requirement in physics is that the predictions of a theory should correspond approximately to experiments; any theory that does not satisfy this requirement can be regarded as providing unphysical results. The lack of numerical structure for $M \in (M_1, M_2)$ and the differences with respect to the experiment shown in Fig. 6(a) by the Maxwell-Cattaneo system are at odds with experiments, and therefore the use of the adjective "unphysical" seems appropriate. The DSMC simulations given in Figs. 5(b)–7 provide additional support to the use of it. However, the term is also used when a theory contradicts an established law of nature or, in the case of hydrodynamics, when the solution turns out to be unstable in the sense of hydrodynamics.

IV. FINAL REMARKS

The shock wave profiles given by the Maxwell-Cattaneo relaxation equations are in good agreement with experiments when the Mach number is lower than about $M_1 \approx 1.2716$; this is one instance where we have found numerical shock wave solutions. The comparisons with the DSMC simulations are also good in this region. As the Mach number is increased from 1, the Maxwell-Cattaneo profiles become narrower, as shown in Fig. 4(a); it may be expected that the lack of solutions found for $M \in (M_1, M_2)$ could be somehow related to this behavior. However, the results shown in Fig. 4 for $M = 1.35$ indicate that, although a numerical shock wave solution does not exist, the piece of the Maxwell-Cattaneo normalized density profile that can be calculated is in relatively good agreement with the DSMC simulations. This suggests that the apparent lack of a standard numerical solutions for Mach numbers slightly greater than $M = 1.2716$ is not a problem about the profiles becoming narrower. Indeed, the problem is near downflow where the derivatives may become infinite or discontinuous at some point so that there is a sort of "resonance" (for the derivatives of the velocity and temperature) phenomena near downflow whose physical meaning is difficult to elucidate because the term responsible for the "resonance" has a complicated structure (see below). We think that the main issue is the "resonant" behavior near downflow where the derivatives become big and even infinite; of course, the Maxwell-Cattaneo ideas are not expected to deal with high gradients, but they generate singularities. On the other hand, the Navier-Stokes equations are also not expected to deal with big gradients but do not have singularities.

For Mach numbers larger than $M = 1.465$ we eventually get a standard numerical shock wave solution for $M = 2$ whose form is rather unusual; see Figs. 4–5. The comparisons with experiments and simulations show that indeed such solution may be considered as "unphysical."

In the Appendix we have obtained the derivatives for the Maxwell-Cattaneo equations without making specific assumptions on the transport coefficients and the relaxation times; the results are

$$\frac{dv^\star}{ds} = \frac{p_3(v^\star, T^\star, T_0^\star, \tau_\sigma^\star, \tau_Q^\star)}{q_1(v^\star, T^\star, T_0^\star, \tau_\sigma^\star, \tau_Q^\star)}, \quad \frac{dT^\star}{ds} = \frac{p_4(v^\star, T^\star, T_0^\star, \tau_\sigma^\star, \tau_Q^\star)}{q_1(v^\star, T^\star, T_0^\star, \tau_\sigma^\star, \tau_Q^\star)}, \tag{30}$$

where the form of the functions p_3 and p_4 are given in the Appendix, and q_1 (responsible for the "resonance") is given by

$$\begin{aligned} q_1 &\equiv q_1(v^\star, T^\star, T_0^\star, \tau_\sigma^\star, \tau_Q^\star) \\ &= -5\tau_\sigma^\star \tau_Q^\star v^{\star 3} + [2(1 + T_0^\star)\tau_\sigma^\star \tau_Q^\star + 2E\kappa^\star \tau_\sigma^\star + 3\eta^\star \tau_Q^\star] v^{\star 2} \\ &\quad + (3T^\star \tau_\sigma^\star \tau_Q^\star - 2E\eta^\star \kappa^\star) v^\star - 2E\tau_\sigma^\star \kappa^\star T^\star. \end{aligned} \tag{31}$$

Here $\tau_A^\star = 3\rho_0 v_0^2 \tau_A/(4\eta_0)$, $A = \sigma, Q$, and $E = 3m\kappa_0/(4k_B\eta_0)$. We have been unable to extract from the previous equation a simpler condition for the appearance of the "resonance," in part for the several quantities present in the equation; in principle, Eq. (31) can be used to model the relaxation times if one is interested in avoiding the "unphysical" solutions. For low Mach numbers our calculations show that sensible profiles can be obtained; such cases correspond to $q_1 > 0$, and this suggests that a good criterion when modeling the relaxation times is to guarantee that $q_1 > 0$ always since this will eliminate the problems found here.

On the other hand, the thermodynamic assumptions used in this work are the following: Concepts such as temperature, internal energy, and pressure can be used in the region between the thermodynamics equilibrium parts of the shock wave that is outside thermodynamic equilibrium. The equation of state for the pressure p and the caloric equation of state for the specific internal energy e [see Eq. (5)] have the same form in the front shock as in thermodynamic equilibrium. We did not use the concept of entropy because the question, what is entropy in nonequilibrium? has several possible answers; see for example the discussion in Ref. [16] regarding two different entropies. Further discussions on entropy and the entropy condition are available [78–80]. The results obtained here are independent of any specific definition of the entropy because no use of the concept was made.

The assumptions just mentioned seem to be sound, at least for Mach numbers near 1, so that the failure of the Maxwell-Cattaneo dynamical system is most likely due to the modeling of the relaxation times and not to the assumptions mentioned above; this is further assured when considering the hyperbolic branch discussed below.

An important requirement in hydrodynamics is that the solution should be stable [2,81] since otherwise it cannot be observed. Actually, it has been pointed out as an objection to the Burnett equations (a representative of the normal solutions branch) since they predict that a fluid at rest is temporarily unstable [82]; for another interpretation see Ref. [83]. Landau and Lifshitz [2] analyzed the case of separation of the stream lines of an ideal fluid at the boundaries of a solid object and argued that the problem of uniqueness for the solution of an ideal fluid (one without dissipation) that arises when separation is present is actually solved by the boundary layer formed when there is viscosity (dissipation), however small. They mentioned that the solutions with separation must be rejected since separation leads to turbulence [2,84]; in other words, the flow will be unstable. For a discussion of the several mechanisms of hydrodynamic instability see Ref. [81]. There are experimental studies of unsteadiness (instability of a steady state) by shock-induced separation in a $M = 2$ compression ramp with air, where coherent structures and turbulence are observed [85], pointing out the importance of shock

interaction with the boundaries. However, the experiments by Alsmeyer, Garen *et al.*, and others [72–74,86] have not reported evidence of these phenomena or other causes of instability in noble gases even for Mach numbers up to 9. The experiments that we have considered here provide stable shock waves so that the Maxwell-Cattaneo should be stable to be physically acceptable. A study of this requires a temporal analysis of Maxwell-Cattaneo equations; if it turned out that they were unstable, this would only deepen the fact that they produce "unphysical" solutions in some cases. Nonlinear stability studies for plane shock waves described by viscous conservations laws are available [78–80].

Finally, we would like to mention briefly other approaches to the shock wave problem in dilute gases. There are two main lines of attempts to study the problem that for convenience we classify as follows:

(1) The normal solutions branch. Here we consider the normal solutions to the Boltzmann equation exemplified by the Chapman-Enskog method [10]. Along this line we can mention the following:

(a) The Navier-Stokes equations [10].

(b) The Burnett, super-Burnett equations, and their variants [10,21,25,28,31–33,37,40].

(c) Generalized Burnett equations [41].

(d) Regularizations of the Burnett equations [34,35].

(2) The moment method, or hyperbolic, branch. We consider here the moment solutions to the Boltzmann equation exemplified by Grad's 13-moment method. In this line we can mention the following:

(a) Grad's 13-moment equations [12].

(b) Extended thermodynamics solutions [7,15–19,49].

(c) Regularized moment equations [21,22,67].

(d) Eu's moment method [20,46,61].

Apart from the attempts mentioned above we have the Mott-Smith method and its variants [23,40], the two-velocity hydrodynamics by Brenner [38,43,62], the finite volume scaling by Margolin [63,64], and the two-fluid hydrodynamics [2,14], among others [5,24,30,36,40,42,43]. A discussion about the attempts mentioned will require a review so that we focus our attention on the hyperbolic branch that is closely related with the Maxwell-Cattaneo system studied here though the Burnett-Cattaneo equations [42] are a hybrid method belonging to both branches.

In 1952 Grad [12] showed that his 13-moment method, when applied to the shock wave problem, failed to provide structure for Mach numbers greater or equal than $M = 1.65$. Holway [15] claimed that for the moment method for solving the Boltzmann equation there exists a critical Mach number beyond which no shock wave solution is possible; Holway's statement has been challenged by Weiss [19]. Jou and Pavón [16] included nonlinear and nonlocal effects into extended thermodynamics, and mentioned that the maximum Mach number above which no shock wave solutions exist can be extended to $M = 4.67$. Ruggeri [17] challenged the result by Jou and Pavón and mentioned that for a generic dissipative hyperbolic system of balance laws there is an upper bound such that for a shock velocity greater than this limit no continuous shock wave structure solutions are possible. Weiss studied the shock wave problem using moment equations with 13, 14, 20, and 21 moments; he concluded that shock wave solutions exist up to certain Mach number that depends on the number of moments used, and quoted the value $M = 1.887$ when using 21 moments. Al-Ghoul and Eu [20] used Eu's moment method [61] and concluded that they could obtain shock wave profiles for all Mach numbers and that their results were in good agreement with the experiments; furthermore, they also claimed that their thermodynamic theory was consistent. For a recent analysis of the shock wave problem using Eu's ideas see Ref. [46]. Torrilhon and Struchtrup [21,22] used a method developed by them called the regularized 13-moment (R13) equations to study the shock wave problem. They provided several comparisons with experiments and DSMC simulations as well as various methods of the normal solution branch; for example, they considered the asymmetry factor obtaining relatively good agreement DSMC and experiments. Among their conclusions is that the quantitative features of the shock are captured by their method for Mach numbers up to $M \approx 3$, and qualitative for higher Mach numbers. Recently Timokhin *et al.* [48] extended the study of the regularized 13-moment equations for the shock wave problem up to Mach numbers $M = 8$, and discussed in particular the overshoot (no monotonicity) in the temperature finding that the two forms of R13 moment equations considered by them (linear and nonlinear) overestimate the overshoot.

There are two main points that we would like to bring to the fore. The first one is that the lack of shock wave solutions is common when considering theories that have a maximum speed of transmission above which no shock wave solutions exist; the case considered in this work fits into this category. The second is that among the theories in the hyperbolic branch Eu's moment method and the R13 moment equations provide shock wave structure for a wide range of Mach numbers. Unfortunately, Eu's theory has not been studied with great detail and in particular studies about the asymmetry factor or the temperature overshoot that is observed in DSMC simulations [29] are missing. On the other hand, the hybrid method (Burnett-Cattaneo) proposed by Holian, Mareschal, and Ravelo [42] that has been claimed to be in quantitative agreement with nonequilibrium molecular-dynamics simulations for strong shocks is another interesting option. However, for the case of strong shocks, with Mach numbers exceeding 100 or so, one must include high-temperature processes [6] such as ionization and electronic excitation among other phenomena; in this case the comparisons with theories that do not include the phenomena mentioned above are of academic interest.

While the numerical computations done are unable to find a standard numerical solution to the Maxwell-Cattaneo equations in some cases, this does not imply that there is not a strong solution or a weak one (solution in the sense of distributions [87,88]). Similarly, while we have been able to find a numerical solution for Mach numbers near 1, this does not mean that there is indeed a solution, either strong or weak, since no use of the Conley index [89] or other mathematical approaches has been considered [78–80]. The relevance of weak solutions nowadays can be exemplified by Fefferman's description [90] of the $1 000 000 (US) prize voiced by the Clay Mathematics Institute for the existence problem of the Navier-Stokes equations. The prize is for smooth solutions, but as Fefferman pointed out: Leray's existence theorem of weak solutions to the Navier-Stokes equations is a good starting point [91].

It is disappointing that, for Mach numbers around $M = 2$, the sound ideas by Maxwell and Cattaneo regarding the lags between "cause" and "effect" (causality) turn out to be bad when compared with experiments and the comoving derivative for the stress and heat flux is used. On the other hand, the use of the partial derivative with respect to time, instead of the comoving derivative, for the fluxes gives the same results as the Navier-Stokes equations for the steady situation here considered. A study of weak solutions or other alternatives to strong solutions may provide an alternative view of what the present work reveals.

Our conclusions with respect to the Maxwell-Cattaneo ideas are for dilute gases, but a similar result (existence of singularities that imply no shock wave solution) holds also for dense gases with constant transport coefficients and relaxation times [8], where the Grüneisen's ideas [6,9] for the equation of state are used. It seems that one must proceed with caution when using the Maxwell-Cattaneo model in other situations, at least for shock waves.

ACKNOWLEDGMENTS

I am grateful for comments from Wm. G. Hoover, E. Pérez-Chavela, and R. M. Velasco.

APPENDIX

In this appendix we obtain the differential equations for the Maxwell-Cattaneo system in a form that does not depend on the explicit form of the relaxation times used in the main text. This is done because the equations are simple to analyze in order to get an idea of what is the main reason why the problems discussed in the paper arise; besides, it is convenient to obtain, by considering particular cases, the equations used by other means.

In terms of reduced variables given by Eq. (8), Eqs. (7) can be expressed as

$$\sigma^\star + \tau_\sigma^\star v^\star \frac{d\sigma^\star}{ds} = \eta^\star \frac{dv^\star}{ds}, \quad \text{with} \quad \tau_\sigma^\star \equiv \frac{3}{4}\frac{\rho_0 v_0^2 \tau_\sigma}{\eta_0}, \tag{A1a}$$

and

$$Q^\star + \tau_Q^\star v^\star \frac{dQ^\star}{ds} = -E\kappa^\star \frac{dT^\star}{ds}, \quad \text{with} \quad \tau_Q^\star \equiv \frac{3}{4}\frac{\rho_0 v_0^2 \tau_Q}{\eta_0} \quad \text{and} \quad E \equiv \frac{3}{4}\frac{\kappa_0 m}{k_B \eta_0}. \tag{A1b}$$

Substitution of Eq. (17a) in Eq. (A1a) and using the second equality that appears in Eq. (17b) into Eq. (A1b) leads to

$$\frac{dv^\star}{ds} = \frac{p_3(v^\star, T^\star, T_0^\star, \tau_\sigma^\star, \tau_Q^\star)}{q_1(v^\star, T^\star, T_0^\star, \tau_\sigma^\star, \tau_Q^\star)}, \quad \frac{dT^\star}{ds} = \frac{p_4(v^\star, T^\star, T_0^\star, \tau_\sigma^\star, \tau_Q^\star)}{q_1(v^\star, T^\star, T_0^\star, \tau_\sigma^\star, \tau_Q^\star)}, \tag{A2}$$

where

$$\begin{aligned} p_3(v^\star, T^\star, T_0^\star, \tau_\sigma^\star, \tau_Q^\star) &= (\tau_\sigma^\star + 3\tau_Q^\star)v^{\star 3} - [2E\kappa^\star + 2(1+T_0^\star)\tau_\sigma^\star + 3(1+T_0^\star)\tau_Q^\star]v^{\star 2} \\ &\quad + [2E(1+T_0^\star)\kappa^\star + (-3T^\star + 5T_0^\star + 1)\tau_\sigma^\star + 3T^\star\tau_Q^\star]v^\star - 2ET^\star\kappa^\star, \end{aligned} \tag{A3a}$$

$$\begin{aligned} p_4(v^\star, T^\star, T_0^\star, \tau_\sigma^\star, \tau_Q^\star) &= (2\tau_Q^\star - \tau_\sigma^\star)v^{\star 4} + [\eta^\star + 2(1+T_0^\star)\tau_\sigma^\star - 4(1+T_0^\star)]v^{\star 3} \\ &\quad + \{-2(1+T_0^\star)\eta^\star + (4T^\star - 5T_0^\star - 1)\tau_\sigma^\star + 2[T^\star + (1+T_0^\star)^2]\tau_Q^\star\}v^{\star 2} \\ &\quad - [(3T^\star - 5T_0^\star - 1)\eta_r + 2T^\star(1+T_0^\star)(\tau_\sigma^\star + \tau_Q^\star)]v^\star + (-3T^{\star 2} + T^\star + 5T^\star T_0^\star)\tau_\sigma^\star, \end{aligned} \tag{A3b}$$

$$q_1(v^\star, T^\star, T_0^\star, \tau_\sigma^\star, \tau_Q^\star) = -5\tau_\sigma^\star\tau_Q^\star v^{\star 3} + [2(1+T_0^\star)\tau_\sigma^\star\tau_Q^\star + 2E\kappa^\star\tau_\sigma^\star + 3\eta^\star\tau_Q^\star]v^{\star 2} + (3T^\star\tau_\sigma^\star\tau_Q^\star - 2E\eta^\star\kappa^\star)v^\star - 2E\tau_\sigma^\star\kappa^\star T^\star. \tag{A3c}$$

Taking $\tau_\sigma^\star$ and $\tau_Q^\star$ equal to zero in Eqs. (A2) and (A3) reproduces the reduced Navier-Stokes equations, see Eq. (16), and using

$$E = \frac{45}{16}, \quad \kappa^\star = \eta^\star, \quad \tau_\sigma^\star = \frac{3}{4}\frac{\eta^\star v^\star}{T^\star}, \quad \tau_Q^\star = \frac{9}{8}\frac{\eta^\star v^\star}{T^\star}, \tag{A4}$$

we obtain Eqs. (14) and (15).

[1] I. G. Currie, *Fundamental Mechanics of Fluids* (McGraw-Hill, New York, 1974).
[2] L. D. Landau and E. M. Lifshitz, *Fluid Mechanics* (Pergamon Press, Oxford, 1986).
[3] J. H. Spurk and N. Aksel, *Fluid Mechanics* (Springer-Verlag, Berlin, 2008).
[4] S. R. de Groot and P. Mazur, *Non-Equilibrium Thermodynamics* (Dover, New York, 1984).
[5] B. L. Holian, C. W. Patterson, M. Mareschal, and E. Salomons, Modeling shock waves in an ideal gas: Going beyond the Navier-Stokes level, Phys. Rev. E **47**, R24 (1993).
[6] Ya. B. Zel'dovich and Yu. P. Raizer, *Physics of Shock Waves and High-Temperature Hydrodynamic Phenomena* (Dover, New York, 2002).
[7] D. Jou, J. Casas-Vázquez, and G. Lebon, *Extended Irreversible Thermodynamics*, 2nd ed. (Springer-Verlag, Berlin, 1993).

[8] F. J. Uribe, Wm. G. Hoover, and C. G. Hoover, Maxwell and Cattaneo's time-delay ideas applied to shock waves and the Rayleigh-Bénard problem, Comput. Methods Sci. Technol. **19**, 5 (2013).

[9] Wm. G. Hoover and C. G. Hoover, Well-posed two-temperature constitutive equations for stable dense fluid shock waves using molecular dynamics and generalized Navier-Stokes-Fourier continuum mechanics, Phys. Rev. E **81**, 046302 (2010).

[10] S. Chapman and T. G. Cowling, *The Mathematical Theory of Non-Uniform Gases* (Cambridge University Press, Cambridge, 1970).

[11] I. Müller and T. Ruggeri, *Extended Thermodynamics* (Springer-Verlag, New York, 1993).

[12] H. Grad, The profile of a steady plane shock wave, Commun. Pure Appl. Math. **5**, 257 (1952).

[13] D. Gilbarg and D. Paolucci, The structure of shock waves in the continuum theory of fluids, J. Ration. Mech. Anal. **2**, 617 (1953).

[14] P. Glansdoff, Solution of the Boltzmann equations for strong shock waves by the two-fluid model, Phys. Fluids **5**, 371 (1962).

[15] L. H. Holway, Existence of kinetic theory solutions to the shock structure problem, Phys. Fluids **7**, 911 (1964).

[16] D. Jou and D. Pavón, Nonlocal and nonlinear effects in shock waves, Phys. Rev. A **44**, 6496 (1991).

[17] T. Ruggeri, Breakdown of shock-wave-structure solutions, Phys. Rev. E **47**, 4135 (1993).

[18] W. Weiss, Continuous shock structure in extended thermodynamics, Phys. Rev. E **52**, R5760 (1995).

[19] W. Weiss, Comments on "Existence of kinetic theory solutions to the shock structure problem" [Phys. Fluids 7, 911 (1964)], Phys. Fluids **8**, 1689 (1996).

[20] M. Al-Ghoul and B. C. Eu, Generalized hydrodynamics and shock waves, Phys. Rev. E **56**, 2981 (1997).

[21] M. Torrilhon and H. Struchtrup, Regularized 13-moment equations: Shock structure calculations and comparison to Burnett models, J. Fluid Mech. **513**, 171 (2004).

[22] H. Struchtrup, *Macroscopic Transport Equations for Rarefied Gas Flows* (Springer-Verlag, Berlin, 2005).

[23] H. M. Mott-Smith, The solution of the Boltzmann equation for a shock wave, Phys. Rev. **82**, 885 (1951).

[24] R. Gatinol, Kinetic theory for a discrete velocity gas and application for the shock structure, Phys. Fluids **18**, 153 (1975).

[25] K. A. Fiscko and D. R. Chapman, Comparison of Burnett, super-Burnett, and Monte Carlo solutions for hypersonic shock structure, in *Rarefied Gas Dynamics*, edited by E. P. Muntz, D. P. Weaver, and D. H. Campbell, Vol. 18 (AIAA, Washington, DC, 1989), pp. 374–395.

[26] G. C. Pham-Van-Diep, D. A. Erwin, and E. P. Muntz, Testing continuum descriptions of low-Mach-number shock structures, J. Fluid Mech. **232**, 403 (1991).

[27] A. N. Gorban and I. V. Karlin, Thermodynamic parametrization, Physica A **190**, 393 (1992).

[28] X. Zhong, R. W. MacCormack, and D. R. Chapman, Stabilization of the Burnett equations and applications to hypersonic flows, AIAA J. **31**, 1036 (1993).

[29] G. A. Bird, *Molecular Gas Dynamics and the Direct Simulation of Gas Flows* (Oxford-Clarendon, New York, 1994).

[30] C. Cercignani, A. Frezzotti, and P. Grosfils, The structure of an infinitely strong shock wave, Phys. Fluids **11**, 2757 (1999).

[31] F. J. Uribe, R. M. Velasco, and L. S. García-Colín, Burnett Description of Strong Shock Waves, Phys. Rev. Lett. **81**, 2044 (1998).

[32] F. J. Uribe, R. M. Velasco, L. S. García-Colín, and E. Díaz-Herrera, Shock wave profiles in the Burnett approximation, Phys. Rev. E **62**, 6648 (2000).

[33] R. K. Agarwal, K.-Y. Yun, and R. Balakrishnan, Beyond Navier-Stokes: Burnett equations for flows in the continuum-transition regime, Phys. Fluids **13**, 3061 (2001).

[34] S. Jin and M. Slemrod, Regularization of the Burnett equations via relaxation, J. Stat. Phys. **103**, 1009 (2001).

[35] K. Xu, Regularization of the Chapman-Enskog expansion and its description of shock structure, Phys. Fluids **14**, L17 (2002).

[36] K. Xu and E. Josyula, Multiple translational temperature model and its shock structure solution, Phys. Rev. E **71**, 056308 (2005).

[37] L. H. Söderholm, Hybrid Burnett equations: A new method of stabilizing, Trans. Theory Stat. Phys. **36**, 495 (2007).

[38] C. Greenshields and J. M. Reese, The structure of shock waves as a test of Brenner's modifications to the Navier-Stokes equations, J. Fluid Mech. **580**, 407 (2007).

[39] Y. Gan, A. Xu, G. Zhang, X. Yu, and Y. Li, Two-dimensional lattice Boltzmann model for compressible flows with high Mach number, Physica A **387**, 1721 (2008).

[40] L. S. García-Colín, R. M. Velasco, and F. J. Uribe, Beyond the Navier-Stokes equations: Burnett hydrodynamics, Phys. Rep. **465**, 149 (2008).

[41] A. V. Bobylev, M. Bisi, M. P. Cassinari, and G. Spiga, Shock wave structure for generalized Burnett equations, Phys. Fluids **23**, 030607 (2011).

[42] B. L. Holian, M. Mareschal, and R. Ravelo, Burnett-Cattaneo continuum theory for shock waves, Phys. Rev. E **83**, 026703 (2011).

[43] F. J. Uribe, The shock wave problem revisited: The Navier-Stokes equations and Brenner's two-velocity hydrodynamics, in *Coping with Complexity: Model Reduction and Data Analysis*, edited by A. N. Gorban and D. Roose (Springer-Verlag, Berlin, 2011), pp. 207–229.

[44] L. Wu, C. White, T. J. Scanlon, J. M. Reese, and Y. Zhang, Deterministic numerical solutions of the Boltzmann equation using the fast spectral method, J. Comput. Phys. **250**, 27 (2013).

[45] N. Frapolli, S. S. Chikatamarla, and I. V. Karlin, Multispeed entropic lattice Boltzmann model for thermal flows, Phys. Rev. E **90**, 043306 (2014).

[46] R. S. Myong, On the high Mach number shock structure singularity caused by overreach of Maxwellian molecules, Phys. Fluids **26**, 056102 (2014).

[47] Z. Guo, R. Wang, and K. Xu, Discrete unified gas kinetic scheme for all Knudsen number flows. II. Thermal compressible case, Phys. Rev. E **91**, 033313 (2015).

[48] M. Yu. Timokhin, Ye. A. Bondar, A. A. Kokhanchik, M. S. Ivanov, I. E. Ivanov, and I. A. Kryukov, Study of the shock wave structure by regularized Grad's set of equations, Phys. Fluids **27**, 037101 (2015).

[49] S. S. Simić, Shock structure in continuum models of gas dynamics: Stability and bifurcation analysis, Nonlinearity **22**, 1337 (2009).

[50] J. C. Maxwell, On the dynamical theory of gases, Philos. Trans. R. Soc. London **157**, 49 (1867).

[51] M. C. Cattaneo, Sur une forme de l'équation de la chaleur éliminant le paradoxe d'une propagation instantaneé, Comptes Rendus de l' Académie des Sciences **247**, 431 (1958).
[52] M. C. Joseph and D. D. L. Preziosi, Heat Waves, Rev. Mod. Phys. **61**, 41 (1989).
[53] C. I. Christov and P. M. Jordan, Heat Conduction Paradox Involving Second-Sound Propagation in Moving Media, Phys. Rev. Lett. **94**, 154301 (2005).
[54] L. S. García-Colín and F. J. Uribe, Extended irreversible thermodynamics beyond the linear regime: A critical overview, J. Non-Equilib. Thermodyn. **16**, 89 (1991).
[55] R. Zwanzig, Memory effects in irreversible thermodynamics, Phys. Rev. **124**, 983 (1961).
[56] B. D. Coleman and M. E. Gurtin, Thermodynamics with internal state variables, J. Chem. Phys. **47**, 597 (1967).
[57] C. Truesdell, *Rational Thermodynamics* (McGraw-Hill, New York, 1969).
[58] D. N. Zubarev, *Nonequilibrium Statistical Thermodynamics* (Consultants Bureau, New York, 1974).
[59] C. Truesdell and R. G. Muncaster, *Fundamentals of Maxwell's Kinetic Theory of a Simple Monatomic Gas* (Academic Press, New York, 1980).
[60] M. Grmela and H. C. Öttinger, Dynamics and thermodynamics of complex fluids. I. Development of a general formalism, Phys. Rev. E **56**, 6620 (1997).
[61] B. C. Eu, *Nonequilibrium Statistical Mechanics* (Kluwer, Dordrecht, 1998).
[62] H. Brenner, Navier-Stokes revisited, Physica A **349**, 60 (2005).
[63] L. G. Margolin, Finite-scale equations for compressible fluid flow, Philos. Trans. R. Soc. A **367**, 2861 (2009).
[64] L. G. Margolin and D. E. Vaughan, Traveling wave solutions for finite scale equations, Mechanics Research Communications **45**, 64 (2012).
[65] A. N. Gorban and I. V. Karlin, Hilbert's 6th problem: Exact and approximate hydrodynamic manifolds for kinetic equations, Bull. Amer. Math. Soc. **51**, 187 (2014).
[66] X.-J. Gu and D. R. Emerson, A high-order moment approach for capturing nonequilibrium phenomena in the transition regime, J. Fluid Mech. **636**, 177 (2009).
[67] M. Torrilhon, Modeling nonequilibrium gas flow based on moment equations, Annu. Rev. Fluid Mech. **48**, 429 (2016).
[68] R. M. Velasco and L. S. García-Colín, Kinetic approach to generalized hydrodynamics, Phys. Rev. A **44**, 4961 (1991).
[69] R. M. Velasco and L. S. García-Colín, The kinetic foundations of extended irreversible thermodynamics revisited, J. Stat. Phys. **69**, 217 (1992).
[70] J. Kestin, K. Knierim, E. A. Mason, B. Najafi, S. T. Ro, and M. Waldman, Equilibrium and transport properties of the noble gases and their mixtures at low density, J. Phys. Chem. Ref. Data **13**, 229 (1984).
[71] T. Scalon, E. Roohi, C. White, M. Darbandi, and J. Reese, An open source, parallel DSMC code for rarefied gas flows in arbitrary geometries, Computers and Fluids **39**, 2078 (2010).
[72] H. Alsmeyer, Density profiles in argon and nitrogen shock waves measured by the absorption of an electron beam, J. Fluid. Mech. **74**, 497 (1976).
[73] B. Schmidt, Electron beam density measurements in shock waves in argon, J. Fluid Mech. **39**, 361 (1969).
[74] W. Garen, R. Synofzik, and G. Wortberg, Experimental investigation of the structure of weak shock waves in noble gases, in *Rarefied Gas Dynamics*, edited by J. L. Potter (AIAA, New York, 1977), pp. 519–528.
[75] F. J. Uribe, R. M. Velasco, and L. S. García-Colín, Two kinetic temperature description for shock waves, Phys. Rev. E **58**, 3209 (1998).
[76] J. Guckenheimer and P. Holmes, *Nonlinear Oscillations, Dynamical Systems, and Bifurcations of Vector Fields* (Springer-Verlag, New York, 1985).
[77] R. Maehara, The Jordan Curve Theorem via the Brouwer Fixed Point Theorem, Am. Math. Mon. **91**, 641 (1984).
[78] T.-P. Liu, Nonlinear stability of shock waves for viscous conservation laws, Memoirs of the American Mathematical Society **56**, 1 (1985).
[79] D. Serre, *Systems of Conservation Laws, Vol. 1, Hyperbolicity, Entropies, Shock Waves* (Cambridge University Press, Cambridge, 1999).
[80] D. Serre, *Systems of Conservation Laws, Vol. 2, Geometric Structures, Oscillation, and Mixed Problems* (Cambridge University Press, Cambridge, 2000).
[81] P. G. Drazin and W. H. Reid, *Hydrodynamic Stability* (Cambridge University Press, New York, 1983).
[82] A. V. Bobylev, The Chapman-Enskog and Grad methods for solving the Boltzmann equation, Dokl. Akad. Nauk SSSR **262**, 71 (1982).
[83] F. J. Uribe, R. M. Velasco, and L. S. García-Colín, Bobylev's instability, Phys. Rev. E **62**, 5835 (2000).
[84] P. Holmes, J. L. Lumley, and G. Berkooz, *Turbulence, Coherent Structures, Dynamical Systems, and Symmetry* (Cambridge University Press, Cambridge, 1998).
[85] B. Ganapathisubramani, N. T. Clemens, and D. S. Dolling, Effects of upstream boundary layer on the unsteadiness of shock-induced separation, J. Fluid Mech. **585**, 369 (2007).
[86] E. A. Steinhilper, Electron beam measurements of the shock wave structure, Part 1, The inference of intermolecular potentials from shock structure experiments, Ph.D. thesis, California Institute of Technology, 1972.
[87] L. Schwartz, *Mathematics for the Physical Sciences* (Hermann, Paris, 1966).
[88] R. D. Richtmyer, *Principles of Advanced Mathematical Physics, Volume I* (Springer-Verlag, New York, 1978).
[89] J. Smoller, *Shock Waves and Reaction-Diffusion Equations* (Springer-Verlag, New York, 1994).
[90] C. L. Fefferman, Existence and smoothness of the Navier-Stokes equation, http://www.claymath.org/sites/default/files/navierstokes.pdf.
[91] J. Leray, Sur le mouvement d'un liquide visquex emplissent l'espace, Acta Math. J. **63**, 193 (1934).